1D- and 2D-ESEEM Study of the Semiquinone Radical Q_A^- of Photosystem II

Yiannis Deligiannakis,*,† Jonathan Hanley,‡ and A. William Rutherford‡

Contribution from The Institute of Materials Science, NCSR "Democritos", 15310 Aghia Paraskevi Attikis, Greece, and Section de Bioénergétique, URA CNRS 2096, Département de Biologie Cellulaire et Moléculaire, CEA Saclay, F-91191 Gif-sur-Yvette, France

Received December 7, 1998. Revised Manuscript Received June 14, 1999

Abstract: The semiquinone radical Q_A^- has been studied by Electron Spin−Echo Envelope Modulation (ESEEM) spectroscopy in Photosystem II membranes at various pH values. The observed nuclear modulations have been assigned by the use of two-dimensional Hyperfine Sublevel Correlation Spectroscopy (HYSCORE) and numerical simulations. Two protein ^{14}N nuclei (N_I and N_{II}) were found to be magnetically coupled with the Q_A^- spin, and on the basis of ^{14}N-NQR and ^{14}N-ESEEM data from the literature, N_I is assigned to an amide nitrogen from the protein backbone while N_{II} is assigned to the amino nitrogen, Nδ, of an imidazole. A physical explanation for such couplings is suggested where the coupling occurs through H-bonds from the protein to the carbonyls of the semiquinone. In PSII membranes treated with CN^-, only the N_I coupling is present above pH 8.5 while both N_I and N_{II} couplings are present at lower pH values. In samples treated at high pH to remove the iron, both N_I and N_{II} couplings are present throughout the pH range studied but at pH <6 these couplings strengthen. These results are interpreted in terms of a model based on the structure of the bacterial reaction center and involving two determining factors. (1) The nonheme iron, when present, is liganded to the imidazole that H-bonds to one of the Q_A^- carbonyls. This physical attachment of the imidazole to the iron limits the strength of the H-bond to Q_A^-. (2) A pH-dependent group on the protein controls the strength of the H-bonds to Q_A^-. The pK_a of this group is influenced by the biochemical treatment used to uncouple the iron, being around pH 7.5 in CN^--treated PSII but around pH 6 in high pH-treated PSII. It is proposed that such a pH effect on the H-bond strength exists in untreated PSII and that earlier observations of pH-induced changes in the EPR signal from the semiquinone iron may reflect this change.

Introduction

In the Photosystem II (PSII) reaction center, a plastoquinone-9 (Q_A, the primary acceptor of the iron−quinone complex) is magnetically coupled to a high spin nonheme Fe^{2+} atom ($S = 2$) when it is reduced to the semiquinone.[1−3] A similar semiquinone−iron complex exists in the closely related but better characterized reaction center of the purple photosynthetic bacteria.[4,5] The magnetic coupling results in the EPR (electron paramagnetic resonance) signal of the semiquinone radical being severely broadened and its spin relaxation becoming very fast.

In PSII, the Q_A^- spin can be decoupled from the nonheme iron using two different approaches. First, the removal of the iron can be done by various biochemical methods. The original method of Klimov et al.,[1] using $LiClO_4$ and *o*-phenanthroline, was based on methods first used in the bacterial reaction center.[6] Variations on this approach have been used where wither the sample is pretreated with trypsin[7] or Zn ions are added.[8,9] Recently, a new protocol for decoupling the iron from the semiquinone was reported[10] involving a treatment at high pH which probably also results in iron loss [11b,c] from the reaction center (see the discussion in ref 10). In all of these methods specific efforts to demonstrate the physical absence of the iron has only been reported in one case.[11a]

The second approach for uncoupling the semiquinone−iron complex involves the conversion of the iron from its physiological high-spin form ($S = 2$) to the low-spin ($S = 0$) state by treatment of PSII with high concentrations of CN^- at alkaline pH.[12] Unlike other methods the decoupling of the semiquinone from the iron is reversible in this case.[12]

The decoupling of the semiquinone from the iron has allowed the use of electron magnetic resonance methods to investigate Q_A^-. Recently, electron spin−echo envelope modulation (ESEEM) spectroscopy[17] on Q_A^- in PSII[10,13,14] and both Q_A^- [15,16] and Q_B^- [16] in bacterial reaction centers was reported. Unlike

* Corresponding author.
† The Institute of Materials Science.
‡ Section de Bioénergétique, URA CNRS.

(1) Klimov, V. V.; Dolan, E.; Shaw, E. R.; Ke, B. *Proc. Natl. Acad. Sci. U.S.A.* **1980**, *77*, 7227.
(2) Nugent, J. H. A.; Diner, B. A.; Evans, M. C. W. *FEBS Lett.* **1981**, *124*, 241.
(3) Rutherford, A. W.; Zimmermann, J. L. *Biochim. Biophys. Acta* **1984**, *767*, 168.
(4) Butler, W. F.; Calvo, R.; Fredkin, D. R.; Isaacson, R. A.; Okamura, M. Y.; Feher, G. *Biophys. J.* **1984**, *32*, 967. (b) Debus, R. J.; Feher, G.; Okamura, M. Y. *Biochemistry* **1986**, *25*, 2276.
(5) Prince, R. C.; Tiede, D. M.; Thornber, J. P.; Dutton, P. L. *Biochim. Biophys. Acta* **1977**, *462*, 467.
(6) Feher, G.; Okamura, M. Y. in *The Photosynthetic Bacteria*; Clayton, R. K., Sistrom, W. R., Eds.; Plenum Press: New York, 1978; p 349.
(7) Bernarding, J.; Eckert, H.-J.; Eichler, H. J.; Napiwotzki, A.; Renger, G. *Photochem. Photobiol.* **1994**, *59*, 566.
(8) Akabori, K.; Kuroiwa, S.; Toyoshima, Y. in *Research in Photosynthesis*; Murata, N., Ed.; Kluwer Academic Publishers: Dordrecht: The Netherlands, 1992; Vol. II, p 123.
(9) It has also been reported that iron is lost during the isolation of the PSII complexes from the membrane, e.g., Tang, X.-S.; Diner, B. A. *Biochemistry* **1994**, *33*, 4594.
(10) Deligiannakis, Y.; Jegerschöld, C.; Rutherford, A. W. *Chem. Phys. Lett.* **1997**, *270*, 564.

10.1021/ja984209c CCC: $18.00
Published on Web 08/06/1999

conventional continuous wave (cw) EPR spectroscopy in which spectra are defined by the selection rules $|\Delta m_S| = 1$ and $|\Delta m_I| = 0$, ESEEM spectra are defined by the selection rules $|\Delta m_S| = 1$, $|\Delta m_I| = 1$ for $I = {}^1/_2$ or $|\Delta m_S| = 1$, $|\Delta m_I| = 1, 2$ for $I = 1$.[17] Thus, the ESEEM technique allows an accurate estimation of weak nuclear hyperfine couplings,[17] even in powder spectra, and in favorable circumstances, the identity of the interacting nuclei and their chemical environment can be determined.[17] Thus, ESEEM can provide detailed information concerning the interactions of the Q_A^- with its immediate environment, and this can be important for understanding of electron transfer to and from this cofactor.

The ESEEM studies of semiquinones in photosynthetic reaction centers showed that the electron spin interacted magnetically with protein nitrogens.[10,13−16,18] In most cases it was assumed that these interactions occurred through hydrogen bonds between the carbonyls of the semiquinone and the protein.[10,13,15,16] A priori this seemed a somewhat unexpected result since ENDOR data for Q_A^- showed that, in all cases, the unpaired electron spin density on the hydrogens involved in the H-bonding was negligible.[19,20] No detailed discussion of the physical basis for the existence of spin density on the nitrogens has yet been given.

In PSII, the number of the ^{14}N nuclei interacting with Q_A^- appears to depend on the biochemical protocol employed to decouple the semiquinone from the iron. In $LiClO_4$/Zn-treated PSII[13] and in PSII treated at pH 11,[10] there are *two* ^{14}N interacting nuclei, and from their nuclear quadrupole interaction (NQI) parameters, these were assigned to the backbone peptide nitrogen (N_I) and the amino nitrogen Nδ of an imidazole (N_{II}).[10,13] On the basis of amino acid sequence analysis and comparison to the crystal structure of the bacterial reaction center,[21] N_I and N_{II} were proposed to belong to the residues Ala261 and His215 of the D2 protein, respectively.[10,13] Equivalent assignments were proposed to explain the couplings detected by ESEEM of Q_A^- in bacterial reaction centers.[15,16]

In ESEEM data for ^{14}N- and ^{15}N-labeled PSII treated with CN at pH 8, only *one* nitrogen coupling was detected.[14] The NQI for this nitrogen corresponded to those of a backbone nitrogen (N_I), and it was assigned to the Ala261 of the D2 protein.[14] More recent ESEEM data[22] provided evidence that in CN-treated PSII, both N_I and N_{II} couplings were present but the N_{II} coupling was weaker than those seen in the preparations with the nonheme iron removed.[22] There was no evident explanation,[22] however, for the absence of these couplings in the original work with CN-treated PSII.[14]

Two other short reports of ESEEM of Q_A^- in PSII also exist in the literature,[23a,b] and the data can be broadly classed into two groups: those done with cyanide and those done without cyanide. In general, the nitrogen couplings detected by ESEEM correspond to those characterized in detail in the studies described above. It should be noted that in one case[23a] the lack of the predicted effects in samples with specifically labeled histidine was taken as indicating that the N_{II} coupling arose from a nonimidazole nitrogen. This contradicts the assignments made by other groups,[10,13,14,22] and the data have been specifically criticized in a recent report.[22] Other data in that work,[23a] however, showed two samples which were treated with CN^- but run at two different pH values (pH 9.2 and 7.8). A feature in the ESEEM spectrum which seems to be attributable to the N_{II} coupling[23a] appears to be somewhat more marked at the lower of the two pH values. In contrast, we reported that, in

(11) Kurreck, J.; Gebers, A.; Reifarth, F.; Andréasson, L.-E.; Parak, F.; Renger, G. *FEBS Lett.* **1987**, *381*, 53. (b) In preparations where Zn^{2+} ions are added, it is sometimes assumed that this ion remains in the site. There is little evidence for this. In a recent study where the iron is displaced from the site by Zn^{2+} or Cu^{2+}, very high concentrations are required, and it is concluded that, when their concentration is lowered in subsequent washing steps, they are lost from the site (Jegerschöld et al., manuscript in preparation). (c) In ref 10, the arguments were given which could be taken as indicating the loss of the iron in the samples treated at pH 11. However the possibility was left open that the high pH treatment resulted in conversion of the iron to the low spin form. Further experimental indications point toward iron loss: No [NO−Fe^{2+}]($S = {}^3/_2$) EPR signal at $g = 4$ (Petrouleas, V.; Diner, B. A. *Biochim. Biophys. Acta* **1990**, *1015*, 131.) can be observed in the pH 11-treated sample. No EPR signal from oxidized Fe^{3+} can be generated under oxidizing conditions, (Deligiannakis, Y. unpublished results.). In contrast, when the low-spin iron is present after CN-treatment, oxidation of the iron results in formation of characteristic $Fe^{3+}(S = {}^1/_2)$ EPR signals (Sanakis, Y.; Petrouleas, V. in *Photosynthesis: From Light to Biosphere*; Mathis, P. Ed.; Kluwer academic Publishers: Dordrecht: The Netherlands, 1995; Vol. I, p 823.). Ongoing Mössbauer experiments of ^{57}Fe-labeled PSII material treated at pH 11 demonstrate the complete absence of high-spin iron (Deligiannakis, Y.; V. Petrouleas, A. W. R.; Andreasson, L. E., to be published). Quantitative estimations, that is, in what percentage of the centers the iron is completely absent, are currently pursued by temperature-dependent Mössbauer spectroscopy.

(12) Sanakis, Y.; Petrouleas, V.; Diner, B. A. *Biochemistry* **1994**, *33*, 9922.

(13) Astashkin, A. V.; Kawamori, A.; Kodera, Y.; Kuroiwa, S.; Akabori, K. *J. Chem. Phys.* **1995**, *102*, 5583.

(14) Deligiannakis, Y.; Boussac, A.; Rutherford, A. W. *Biochemistry* **1995**, *34*, 16030.

(15) Spoyalov, A. P.; Hulsebosch, R. J.; Shochat, S.; Gast, P.; Hoff, A. J. *Chem. Phys. Lett.* **1996**, *263*, 715.

(16) Lendzian, F.; Rautter, J.; Käβ, H.; Gardiner, A.; Lubitz, W. *Ber. Bunsen-Ges. Phys. Chem.* **1996**, *100*, 2036.

(17) Dikanov, S. A.; Tsvetkov, Yu. D. *Electron Spin−Echo Envelope Modulation (ESEEM) Spectroscopy*; CRC Press: Boca Raton, FL, 1992.

(18) Hanley, J.; Deligiannakis, Y.; MacMillan, F.; Bottin, H.; Rutherford, A. W. *Biochemistry* **1997**, *36*, 11543.

(19) MacMillan, F.; Lendzian, F.; Renger, G.; Lubitz, W. *Biochemistry* **1995**, *34*, 8144. (b) Rigby, S.; Nugent J. H. A.; Evans M. C. W. *Biochemistry* **1995**, *34*, 12075. (c) Zeng, M.; Dismukes, G. C. *Biochemistry* **1996**, *35*, 8955.

(20) Lubitz, W.; Abresch, E. C.; Debus, R. J.; Isaacson, R. A.; Okamura, M. Y.; Feher, G. *Biochim. Biophys. Acta* **1985**, *808*, 464. (b) Feher, G.; Isaacson, R. A.; Okamura, M. Y.; Lubitz, W. In *Antennas and Reaction Centres of Photosynthetic Bacteria*; Michel-Beyrle, M. E., Ed., Springer, Berlin, Germany, 1996; Vol. 42, p 353.

(21) Michel, H.; Deisenhofer, J. *Biochemistry* **1988**, *27*, 1. (b) Trebst, A. *Z. Naturforsch., C: Biosci.* **1991**, *46*, 557. (c) Ermler, U.; Fritzsch, G.; Buchanan, G. S. K.; Michel, H. *Curr. Biol.* **1994**, *2*, 925. (d) Rutherford A. W. In *Progress in Photosynthesis Research*; Biggins, J., Ed.; Martinus Nijhoff Publishers: Dordrecht, The Netherlands, 1987; Vol. I. p 235.

(22) Astashkin, A. V.; Kuroiwa, S.; Kawamori, A.; Akabori, K. *J. Chem. Phys.* **1998**, *108*, 10143.

(23) Tang, X.-S.; Peloquin, J. M.; Lorigan, G. A.; Britt, R. D.; Diner, B. A. In *Photosynthesis: From Light to Biosphere*; Mathis, P. Ed.; Kluwer Academic Publishers: Dordrecht, The Netherlands, 1995; Vol. I, p 775. (b) MacMillan, F.; Kurreck, J.; Lendzian, F.; Käss, H.; Reifarth, F.; Renger, G.; Lubitz, W. In *Photosynthesis: From Light to Biosphere*; Mathis, P. Ed.; Kluwer Academic Publishers: Dordrecht, The Netherlands, 1995; Vol. I, p 659. (c) A report of ESEEM of Q_A^- in the presence of high-spin iron $Fe^{2+}(S = 2)$ (i.e., nonmodified PSII) appeared after submission of the present manuscript (Peloquin, J. M.; Tang, X.-S.; Diner, B. A.; Britt, R. D. *Biochemistry* **1999**, *38*, 2057.). It showed that the ESEEM spectra of the intact system closely resemble that of CN-treated at pH 6.3 that we report here. In both cases the ESEEM data indicate that two sets of nitrogens with similar quadrupole and hyperfine couplings are coupled to Q_A^-. This shows that at this pH the environment of the Q_A^- in CN-treated PSII is quite similar to its environment in intact PSII. In the same article the assignment of the N_I coupling (peaks at 0.7, 2.0, 2.85, 5.0 MHz) to a peptide was adopted in line with the earlier work,[23a] but its assignment to alanine 260 was questioned on the basis of site-directed mutagenesis.[23c] The N_{II} features (peaks at 0.6−0.9, 1.6 MHz) assigned earlier to an imidazole nitrogen on the basis of the NQI values (see introduction) remain unassigned in this work. This is based on the earlier observation that His-labeled PSII did not show the expected changes.[23a] As pointed out in the Introduction, this work[23a] has been questioned recently.[22] Furthermore, the strengthening of the N_{II} coupling at low pH reported in the present work results in an ESEEM spectrum which is very characteristic of imidazole.[39a] Indeed similar signals have been described by the same group as characteristic of an imidazole coupling (Eliot, S. J.; Randal, D. W.; Britt, R. D.; Chan, S. I. *J. Am. Chem. Soc.* **1998**, *120*, 3247). Moreover the recent FTIR data[36c] that one of the authors (X.-S. Tang) published on material similar to that used in the ESEEM study clearly shows the presence of H-bond between Q_A^- and His.[36c]

samples treated at pH 11 to decouple the iron,[10] the ^{14}N-couplings to Q_A^- were essentially unaffected by changing the pH from pH 11 to 6.

The determination of the spin-Hamiltonian parameters from the ESEEM spectrum is straightforward in the cases where the hyperfine coupling "matches" the nuclear Larmor frequency, that is, $A \sim 2\nu_I$.[17] In principle, this ideal regime can be always achieved by recording Zeeman-dependent ESEEM spectra at a series of microwave frequencies.[24] Alternatively, in some cases of anisotropic EPR spectra, Zeeman-dependent ESEEM spectra can be recorded across the EPR spectrum; however with narrow EPR spectra, like those of radicals, this option is not applicable. In the case of overlapping ESEEM spectra, that is, due to multiple nuclear coupling, resolution of the various components might be cumbersome even in the "matching" regime. Hyperfine sublevel correlation spectroscopy (HYSCORE)[25a] is a two-dimensional (2D) four-pulse ESEEM technique which provides correlations between nuclear frequencies originating from different *Ms* manifolds.[25a] This technique has proven to be a useful tool for the analysis of overlapping complicated ESEEM spectra.[25b−f] The superiority of HYSCORE for resolving and assigning complicated ESEEM spectra has been demonstrated recently for the case of the pheophytin (Pheo = the intermediate electron acceptor pheophytin) anion of PSII.[25g] Here we report a detailed ESEEM and HYSCORE study of Q_A^- in PSII membranes buffered at various pH values.

Materials and Methods

Sample Preparation. PSII membranes were isolated from market spinach as described previously[26a] with the modifications described in ref 26b and stored in 0.4 M Sucrose, 25 mM MES−NaOH (MES = 2-(*N*-morpholino)-ethanesulfonic acid) (pH 6.5), and 10 mM NaCl (SMN buffer). To convert the iron to the low-spin state, PSII membranes were incubated with 300 mM KCN at pH 8.1.[12,14] In a separate series of experiments, the iron was magnetically decoupled from the quinone by treating PSII membranes at pH 11, according to the protocol described in ref 10. After either of these pretreatments, the PSII membranes were resuspended, washed once in SMN buffer at pH values between 6 and 11, and stored in liquid nitrogen. The buffers used were MES (pH 6−6.5), HEPES (pH 7−8), Tris (tris(hydroxymethym)-aminomethane) (pH 8−8.5), or glycine (pH 9−11). For chemical reduction of the Q_A^-, sodium dithionite was added to the PSII samples to reach a potential of -160 ± 10 mV, followed by incubation in an ice bath in the dark. The redox potential was measured in the sample with a platinum electrode, with a calomel reference electrode described previously.[14]

EPR Spectroscopy. Continuous-wave (cw) EPR spectra were recorded at liquid helium temperatures with a Bruker ER 200 X-band spectrometer equipped with an Oxford Instruments cryostat. The microwave frequency and the magnetic field were measured with a microwave frequency counter HP 5350B and a Bruker ER035M NMR gaussmeter, respectively.

ESEEM Spectroscopy. Pulsed EPR was performed with the Bruker ESP 380 spectrometer equipped with a dielectric resonator and a BRUKER ESP380−1078 IN echo-integrator. The instrument dead-time was about 100 ns. For the field-swept spectra the echo integral was recorded as a function of the magnetic field after a two pulse sequence ($\pi/2$-144 ns-π). The durations of the $\pi/2$ and π pulses were 64 and 128 ns, respectively. In the three-pulse ($\pi/2$-τ-$\pi/2$-T-$\pi/2$) ESEEM spectra, the amplitude of the stimulated echo as a function of $\tau + T$ was measured at a frequency near 9.6 GHz at a magnetic field corresponding to the maximum intensity of the field-swept spectrum. The minimum interpulse T was 56 ns and was incremented in steps of 8 ns. The duration of the $\pi/2$ pulse was 16 ns. 2D-HYSCORE spectra were recorded using the sequence ($\pi/2$-τ-$\pi/2$-t_1-π-t_2-$\pi/2$-echo), where the echo is measured as a function of t_1 and t_2.[25a] The durations of the $\pi/2$ and π pulses were 16 ns and 32 ns respectively, with equal amplitudes. Points (200−240) were recorded in each dimension for a series of τ values between 104 and 360 ns, while the t_1 and t_2 were incremented in steps of 16 ns from their initial value. To remove the unwanted echoes, the appropriate phase-cycling procedures in the stimulated-echo[27a] and HYSCORE[27b] experiments were applied.

Data Manipulation. (i) 1D-Stimulated Echo ESEEM. The experimental spectrum was normalized to the time-zero echo intensity which was estimated by dead-time reconstruction according to Mims.[28] Prior to Fourier transform the time-domain echo decay was factored out by subtraction of a linear function, and zero-filling to 512 points was performed followed by a tapering with a Hamming window. The spectra presented are calculated in the magnitude mode.

(ii) 2D-HYSCORE ESEEM. The background decay in both t_1 and t_2 dimensions was subtracted using a linear function followed by zero-filling to 1024 points in two dimensions and tapering with a Hamming window; then Fourier transform was carried out in both dimensions.

Simulation of ESEEM Spectra. The spin Hamiltonian for an $S = {}^1/_2$, $I = 1$ system with isotropic g factor is

$$H = g\beta \boldsymbol{BS} + g_n\beta_n \boldsymbol{BI} + \boldsymbol{SAI} + \boldsymbol{IQI} \qquad (1)$$

The hyperfine tensor $\boldsymbol{A}$ has principal values (A_{xx}, A_{yy}, A_{zz}). $\mathbf{Q}$ is the nuclear quadrupole tensor; its components in its principal axes system are $Q^P_{zz} = Q/2I(2I-1)$, $Q^P_{xx} = -Q^P_{zz}(1-\eta)/2$, $Q^P_{yy} = -Q^P_{zz}(1+\eta)/2$, where $\eta = (Q^P_{xx} - Q^P_{yy})/Q^P_{zz}$ and $Q = e^2qQ_n/h$ is the quadrupole coupling constant due to a quadrupole moment Q_n interacting with the electric field gradient q at the nucleus. The principal axes systems of the tensors $\mathbf{A}$ and $\mathbf{Q}$ are related by the Euler angles (α, β, γ).[29] Numerical simulations have been performed by calculating the three-pulse ESEEM in the time domain according to the expressions of Mims[30] as described earlier.[25g]

Analysis of the 2D-HYSCORE Spectra. The principal factors determining the HYSCORE spectra for $I = {}^1/_2$,[25g,31,32] $I = 1$,[25d−f] and recently for $I = {}^3/_2$[33] have been analyzed in the literature. Here we briefly reiterate the basic ideas which are pertinent to our discussion. The appearance of the HYSCORE spectrum is sensitive to the relative signs of the nuclear frequencies; a correlation peak at ($\nu_{ij}(\alpha)$, $\nu_{mn}(\beta)$) appears in the (+, +) quadrant, while the correlation peak ($\nu_{ij}(\alpha)$, $-\nu_{mn}(\beta)$) appears in the (+, −) quadrant. The intensities of the cross peaks at ($\nu_{ij}(\alpha)$, $\nu_{mn}(\beta)$) and ($\nu_{ij}(\alpha)$, $-\nu_{mn}(\beta)$) depend on the factors $M_{im}M^*_{jn}$ and $M_{jm}M^*_{in}$, respectively,[25d,33] where the matrix element M_{kn} gives the EPR transition amplitude from the kth sublevel within the α spin manifold to the nth sublevel within the β spin manifold. In general, these intensity factors differ since they are determined by the matrix

(24) Singel, D. J. In *Advanced EPR: Applications in Biology and Biochemistry*; Hoff, A. J., Ed.; Elsevier: Amsterdam, The Netherlands, 1989; p 119.

(25) Höfer, P.; Grupp, A.; Nebenführ, H.; Mehring, M. *Chem. Phys. Lett.* **1986**, *132*, 279. (b) Shane, J. J.; Höfer, P.; Reijerse, E. J.; De Boer, E. J. *J. Magn. Reson.* **1992**, *99*, 596. (c) Käβ, H.; Bittersmann-Weidlich, E.; Andréasson, L.-E.; Bönigk, B.; Lubitz, W. *Chem. Phys.* **1995**, *194*, 419. (d) Dikanov, S. A.; Xun, L.; Karpiel, A. B.; Tyryshkin, A. M.; Bowman, M. K. *J. Am. Chem. Soc.* **1996**, *118*, 8408. (e) Kofman, V.; Shane, J. J.; Dikanov, S. A., Bowman, M. K.; Libman, J.; Shanzer, A.; Goldfarb, D. *J. Am. Chem. Soc.* **1995**, *117*, 12771. (f) Kofman, V.; Farver, O.; Pecht, I.; Goldfarb, D. *J. Am. Chem. Soc.* **1996**, *118*, 1201. (g) Deligiannakis, Y.; Rutherford, A. W. *J. Am. Chem. Soc.* **1997**, *119*, 4471.

(26) Berthold, D. A.; Babcock, G. T.; Yocum, C. F. *FEBS Lett.* **1981**, *134*, 231. (b) Boussac, A.; Rutherford, A. W. *Biochemistry* **1988**, *27*, 3476.

(27) Fauth, J. M.; Schweiger, A.; Braunschweiler, L.; Forrer, J.; Ernst, R. *J. Magn. Reson.* **1986**, *66*, 64. (b) Gemperle, G.; Aebli, G.; Schweiger, A.; Ernst, R. R. *J. Magn. Res.* **1990**, *88*, 241.

(28) Mims, W. B. *J. Magn. Res.* **1984**, *59*, 291.

(29) The Euler angles are defined according to Mathews, J.; Walkers, R. L. *Mathematical Methods of Physics*; W. A. Benjamin, Inc.: New York, 1970; p 404; that is, α is a positive rotation about Z axis, β is a positive rotation about Y' axis, and γ is a positive rotation about Z' axis.

(30) Mims, W. B. *Phys. Rev. B: Solid State* **1972**, *5*, 2409. (b) Mims, W. B. *Phys. Rev. B: Solid State* **1972**, *6*, 3543.

(31) Pöppl, A.; Kevan, L. *J. Phys. Chem.* **1996**, *100*, 3387.

(32) Reijerse, E. J.; Dikanov, S. A. *Pure Appl. Chem.* **1992**, *64*, 789. (b) Dikanov, S. A.; Bowman, M. K. *J. Magn. Res. A* **1995**, *116*, 125.

(33) Deligiannakis, Y.; Astrakas, L.; Kordas, G.; Smith, R. *Phys. Rev. B: Solid State* **1998**, *58*, 11420. (b) Astrakas, L.; Deligiannakis, Y.; Mitrikas, G.; Kordas, G. *J. Chem. Phys.* **1998**, *109*, 8612.

elements describing the four possible transitions between the two levels i and j, and m and n in each M_S manifold. Due to this, the two crosspeaks having the same absolute values of frequencies, but being at opposite quadrants, have different intensities. In the limit of weak hyperfine coupling ($A_{iso} \ll \nu_I$) the crosspeaks at ($\nu_{ij}^{(\alpha)}$, $\nu_{mn}^{(\beta)}$) in the (+, +) quadrant attain maximal intensity relative to the crosspeak at ($\nu_{ij}^{(\alpha)}$, $-\nu_{mn}^{(\beta)}$) which has minimal intensity. In the opposite limit of strong hyperfine coupling ($A_{iso} \gg \nu_I$) it is the crosspeaks in the (+, −) quadrant which have maximum intensity. For intermediate hyperfine couplings, the eigenfunctions have mixed m_I character; in the limiting case of the "exact cancellation", that is, for $A_{iso} = 2\nu_I$, the peaks in both the (+, +) and (+, −) quadrants have comparable intensity.[25d,33]

For a single ^{14}N nucleus, in the case of "exact cancellation",[17,34] the ESEEM spectrum contains three sharp low-frequency lines, with maxima at frequencies given by the relations $\nu_+ = 3(e^2qQ_n/4h)(1 + \eta)$, $\nu_- = 3(e^2qQ_n/4h)(1 - \eta)$, $\nu_0 = 2(e^2qQ_n/4h)\eta$, and a "double-quantum" ($\Delta m_I = 2$) line has maximum intensity at a frequency $\nu_{dq} \approx 2[(\nu_I + A/2)^2 + K^2 (3 + \eta^2)]^{1/2}$ where $K = e^2qQ_n/4h$. In the corresponding 2D-HYSCORE spectrum, correlation peaks at frequency coordinates (ν_0, ν_{dq}), (ν_-, ν_{dq}) and (ν_+, ν_{dq}) are predicted[25d−f] (see Figure 1).

Compared to the correlation peaks at (ν_0, ν_{dq}), (ν_-, ν_{dq}), those at (ν_+, ν_{dq}) are more intense and are most easily detected in experimental ^{14}N−HYSCORE spectra.[25d−f]

In the presence of weak hyperfine anisotropy, that is, compared to A_{iso}, the ν_{dq} feature is broadened to first order due to a distribution of the corresponding transition frequencies.[25d] In the HYSCORE spectrum, the presence of weak hyperfine anisotropy results in a spreading of the (ν_+, ν_{dq}) correlation features which attain elongated shapes.[25d,32] Thus the frequency positions of the correlation peaks in the 2D-HYSCORE spectrum allow an estimation of the nuclear transition frequencies, while their shape provides information about the extent of hyperfine anisotropy.[25d,32]

Results

The cw EPR signal of the Q_A^- radical in PSII when decoupled from the Fe^{2+}($S = 2$) is a derivative with isotropic $g = 2.0045$ and a width of $\Delta H \sim 9.5$ G.[10,13,14,22] A similar EPR signal is recorded for Q_A^- in PSII buffered at pH 6.3 after the CN treatment at pH 8.1 (see inset in Figure 2). Comparable EPR signals are also recorded for Q_A^- in PSII buffered at intermediate pH values between 5 and 9, after the CN treatment at pH 8.1 (not shown). The detection of the free semiquinone EPR signal at all these pH values shows that in all these samples the Q_A^- remains decoupled from the iron.

The resolution of the cw EPR signal for Q_A^- is limited by its inhomogeneous line width, that is, ∼9.5 G; thus magnetic interactions of a few Gauss or less are not resolved by cw EPR. On the other hand, ESEEM spectroscopy allows a high-resolution analysis of weak magnetic interactions.[10,13−17] Representative frequency domain stimulated ESEEM spectra for Q_A^- in CN^--treated PSII at various pH values are displayed in Figure 2.

Before we proceed to the assignment of these ESEEM features, we note that on going from alkaline to more acidic pH, there is a progressive change in certain spectral features, the more prominent being the increase of the intensity of the feature at ∼1.7 MHz.

Our approach for the proper assignment of the observed spectral features was to perform hyperfine sublevel correlation (HYSCORE) experiments. Subsequently, numerical simulations were performed for a more accurate estimation of the coupling parameters.

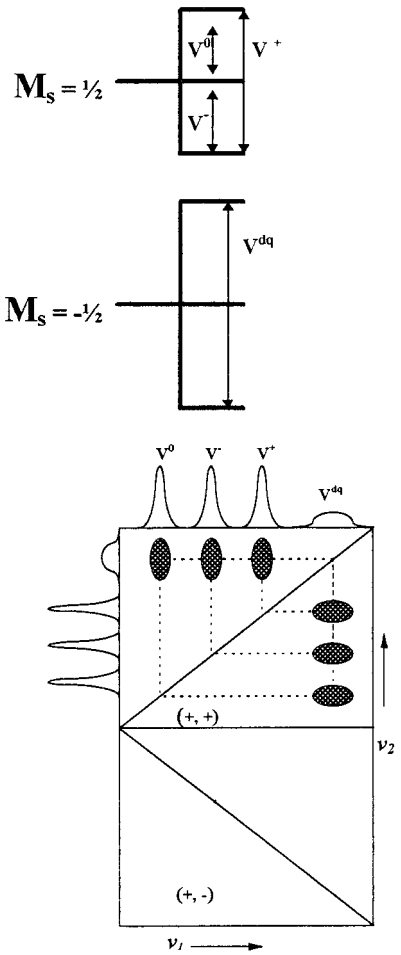

Figure 1. A descriptive view of a 2D-HYSCORE spectrum for a single ^{14}N nucleus coupled to the electron spin with $A_{iso} \sim 2\nu_I$. Only the (+, +) quadrant featured is displayed. The corresponding 3-pulse ESEEM spectrum consists of three NQI lines at ν_0, ν_-, and ν_+ and a broad "double quantum" ν_{dq} line. The expected correlation features are those between the ν_{dq} and the ν_0, ν_-, ν_+ transitions and appear in pairs symmetrically disposed around the diagonal. Typically the pair of crosspeaks at (ν_+, ν_{dq}) and (ν_{dq}, ν_+) is best resolved in experimental HYSCORE spectra.

2D-HYSCORE for Q_A^- in CN-Treated PSII. Representative 2D-HYSCORE spectra for CN-treated PSII at either pH 9.2 or 6.3 are displayed in Figure 3, parts A and B, respectively.

The HYSOCRE spectrum for CN-treated PSII at pH 9.2 (Figure 3A) is dominated by crosspeaks at (2.8 MHz, 5.1 MHz) and (0.8, 5.1 MHz), all in the (+, +) quadrant. This spectrum should be compared with the corresponding HYSCORE spectrum for the Q_A^- at pH 6.3 (Figure 3B), which exhibits additional crosspeaks at (1.7 MHz, 4.0−4.2 MHz); additional crosspeaks at (0.8−1.0 MHz, 4.1 MHz) are also resolved at lower contour levels or in spectra recorded at other τ values. In both spectra, Figure 3, parts A and B, weak crosspeaks are consistently resolved at higher frequencies, that is, at 11.4 and 17.7 MHz in the (+, +) quadrant.

^{14}N Couplings. The low-frequency features below 6 MHz are due to ^{14}N nuclei interacting with the Q_A^- spin. According to the theoretical analysis of the HYSCORE spectra (see also Figure 1), the features at (2.8 MHz, 5.1 MHz) and (0.8 MHz, 5.1 MHz) are assigned to the (ν_+, ν_{dq}) and (ν_0, ν_{dq}) cross-features, respectively, due to one ^{14}N nucleus (N_I) interacting with the electron spin. Accordingly, for $\nu_0 = 0.8$ MHz and $\nu_+ = 2.8$ MHz we may estimate the ν_- frequency for N_I: that is, $\nu_- = \nu_+ - \nu_0 = 2.1$ MHz. From these values, the quadruple

(34) Dikanov, S. A.; Tsvetkov, Y. D.; Bowman, M. K.; Astashkin, A. V. *Chem. Phys. Lett.* **1982**, *90*, 149. (b) Mims, W. B.; Peisach, J. *J. Chem. Phys.* **1978**, *69*, 4921. (c) Flanagan, H., L.; Singel, D. J. *J. Chem. Phys.* **1987**, *87*, 5606. (d) Reijerse, E. J.; Keijzers, C. P. *J. Magn. Res.* **1987**, *71*, 83.

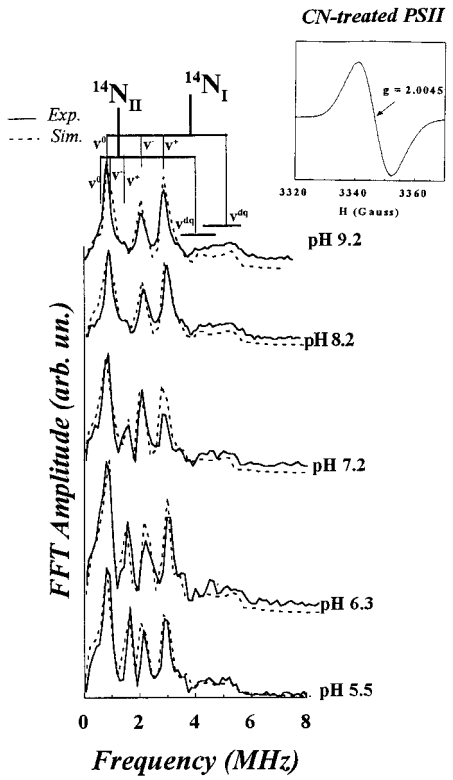

Figure 2. Fourier transform of the 3-pulse ESEEM recorded for Q_A^- in CN-treated PSII buffered at the indicated pH values (solid lines). The simulated spectra (dashed lines) have been calculated by using the coupling parameters listed in Table 1A. The various features are labeled according to their origin. Experimental conditions: $H = 3458$ G; sample temperature, 19 K; $\tau = 104$ ns; time interval between successive pulse sets, 3 ms; and microwave frequency, 9.64 GHz. Inset: X-band cw EPR spectrum of Q_A^- in CN-treated PSII membranes buffered at pH 6.3, in the presence of dithionite. Experimental conditions: sample temperature, 12 K; microwave frequency, 9.415 GHz; microwave power, 32 μW; and modulation amplitude, 2 G.

coupling parameters for $^{14}N_I$ may be estimated from the relations $e^2qQ_n/4h = K = [\nu_+ + \nu_-]/6 \sim 0.82$ MHz and $\eta = \nu_0/2(e^2qQ_n/4h) \sim 0.49$, and by using the relation $\nu_{dq} \approx 2[(\nu_I + A_{iso}/2)^2 + K^2(3 + \eta^2)]^{1/2}$, the hyperfine coupling A_{iso} is estimated to be $\sim$2.0 MHz. We observe that the hyperfine coupling of N_I fulfils the cancellation condition,[34c] $A_{iso} \sim 2\nu_I$, and this results in nuclear transitions at the purely quadruple transitions (ν_-, ν_+, ν_0).[17,34] At pH 6.3, Figure 3B, in addition to the features due to N_I, the strong crosspeaks at (1.7 MHz, 4.0−4.2 MHz) correspond to the (ν_+, ν_{dq}) of a second ^{14}N nucleus (N_{II}) coupled with Q_A^-. The (ν_-, ν_{dq}) feature of N_{II} is at ($\sim$0.9 MHz, 4.0−4.2 MHz), resolved at lower contour levels or HYSCORE spectra recorded at other τ values. By using these values ($\nu_+ \sim$ 1.7 MHz, $\nu_- \sim 0.9$ MHz, $\nu_0 \sim 0.8$ MHz, and an average ν_{dq} of 4.1 MHz), the coupling parameters for N_{II} may be estimated to be $e^2qQ_n/4h \sim 0.35$ MHz and $\eta \sim 0.69$ and $A_{iso} \sim$1.76 MHz. Although the estimated A_{iso} value for N_{II} deviates from the $2\nu_I$ value (i.e., $|A_{iso} - 2\nu_I| = 0.36$ MHz), this deviation does not exceed $4K/3\nu_I \sim 0.8$ MHz, that is, the limiting value for the validity of the cancellation condition.[34c] Therefore, the estimated values for N_{II}, like those for N_I, provide a reliable set of ^{14}N coupling values. These values can be further refined by numerical simulations of the three-pulse ESEEM (see below).

In recapitulating, the HYSCORE data show that in CN-treated PSII the semiquinone Q_A^- is magnetically coupled to two ^{14}N nuclei (N_I and N_{II}) at pH 6.3, while it is magnetically coupled to one ^{14}N nucleus only (N_I) at pH 9.2. At intermediate pH values, that is, pH 8.3 (inset in Figure 3A), although the features due to N_I remain unaltered, both in frequency position and intensity, the crosspeaks due to N_{II} have significantly weaker intensity; essentially only the (ν_+, ν_{dq}) crosspeaks at ($\sim$1.7 MHz, $\sim$3.8 MHz) are resolved. In the HYSCORE spectrum at pH 7.2 and 5.5 (not shown), the ν_{dq} peak is centered at $\sim$3.9 and 4.2 MHz respectively; thus we have a progressive decrease of the frequency of the ν_{dq} crosspeak as a function of the pH, that is, $\langle\nu_{dq}\rangle \sim 4.2$ MHz at pH 5.5, ~ 4.0 MHz at pH 6.3, ~ 3.9 MHz at pH 7.2, and ~ 3.8 MHz at 8.3. When the quadruple coupling values for N_{II} ($K \sim 0.35$, $\eta \sim 0.69$) estimated at pH 6.3 are used, these ν_{dq} values correspond to A_{iso} values of $\sim$1.8 MHz at pH 5.5, decreasing to $\sim$1.6 MHz at pH 6.3, $\sim$1.5 MHz at pH 7.2, and $\sim$1.3 MHz at pH 8.3. This decrease of the ν_{dq} values indicates that increasing pH results in a progressive decrease of the A_{iso} value of N_{II}.

^{1}H Couplings. The high-frequency features which are clustered around the ^{1}H-Larmor frequency ($\sim$14.7 MHz) are due to $^1H(I = 1/2)$ nuclei interacting with the Q_A^- spin. The fact that they have maximum intensity in the (+, +) quadrant of the HYSCORE spectrum indicates that they originate from protons with weak hyperfine coupling $A \ll 2\nu_I$.[25g,31,32] For a proton ($I = 1/2$) with isotropic hyperfine coupling $A_{iso} < \nu_I$, the two nuclear transitions occur at frequencies $\nu_I \pm A_{iso}/2$.[17] Thus, in the HYSCORE spectrum the corresponding cross-features are at ($\nu_I + A_{iso}/2$, $\nu_I - A_{iso}/2$), and their frequency distance allows a direct estimation of the A_{iso} from the spectrum. In the presence of axial hyperfine anisotropy, T, the nuclear transitions occur in the range $\nu_{||} = \nu_I \pm (A_{iso}+2T)/2$ to $\nu_\perp = \nu_I \pm (A_{iso} - T)/2$[17] and the corresponding HYSCORE crosspeaks become arc-shaped ridges[25g,31,32] with a maximum length of $3T$. From the shape of the ^{1}H-ridges in Figure 3, based on earlier work[25g,32b] and taking into account lower contour intensities also, we estimate a ^{1}H-tensor with $A_{iso} \sim 5.7$ MHz and $T < 1.0$ MHz.

In summary, the HYSCORE data show that in CN-treated PSII, pH has a specific effect on the magnetic coupling between the Q_A^- and nitrogen N_{II}, but not N_I. At acidic pH both N_I and N_{II} are coupled to Q_A^-, but the N_{II} coupling is severely weakened at alkaline pH. This observation allows a qualitative, but straightforward, explanation of the changes observed in the 1D-ESEEM spectra in Figure 2 (to facilitate the discussion, the various features in Figure 2 have been labeled according to their origin). At acidic pH, both N_I and N_{II} are coupled with Q_A^-; thus, the ESEEM spectrum at pH 5.5 in Figure 2 contains well resolved features due to N_I (at 2.8, 2.1, 0.8, and 5.0−5.2 MHz) and to N_{II} at (1.7, 0.9, and 4.0−4.3 MHz plus a shoulder at 0.6 MHz at pH 5.5). On going toward more alkaline pH, the N_{II} coupling becomes weaker. At pH values between 7 and 8 the N_{II} features show a steep decrease and finally at pH 9.2 the N_{II} contribution to the ESEEM spectrum is negligible.

To examine the reversibility of the observed pH effects, the sample at pH 6.3 was resuspended at pH 9.2, washed twice, and incubated for 40 min in an ice bath. The corresponding ESEEM spectrum (not shown) for Q_A^- was identical to the ESEEM spectrum for pH 9.2 in Figure 2. In an analogous experiment the ESEEM spectrum of the sample at pH 9.2 was converted to that of the spectrum at pH 6.3 in Figure 2, after changing its pH to this value, that is, 6.3. Thus, the pH effect on the interaction of the Q_A^- with the protein ^{14}N nuclei is reversible.

pH Effect in pH 11-Treated PSII. In the following, we study the ESEEM spectra of Q_A^- in iron-depleted PSII samples by treatment at pH 11.[10] For pH values above pH 5.8, the ESEEM

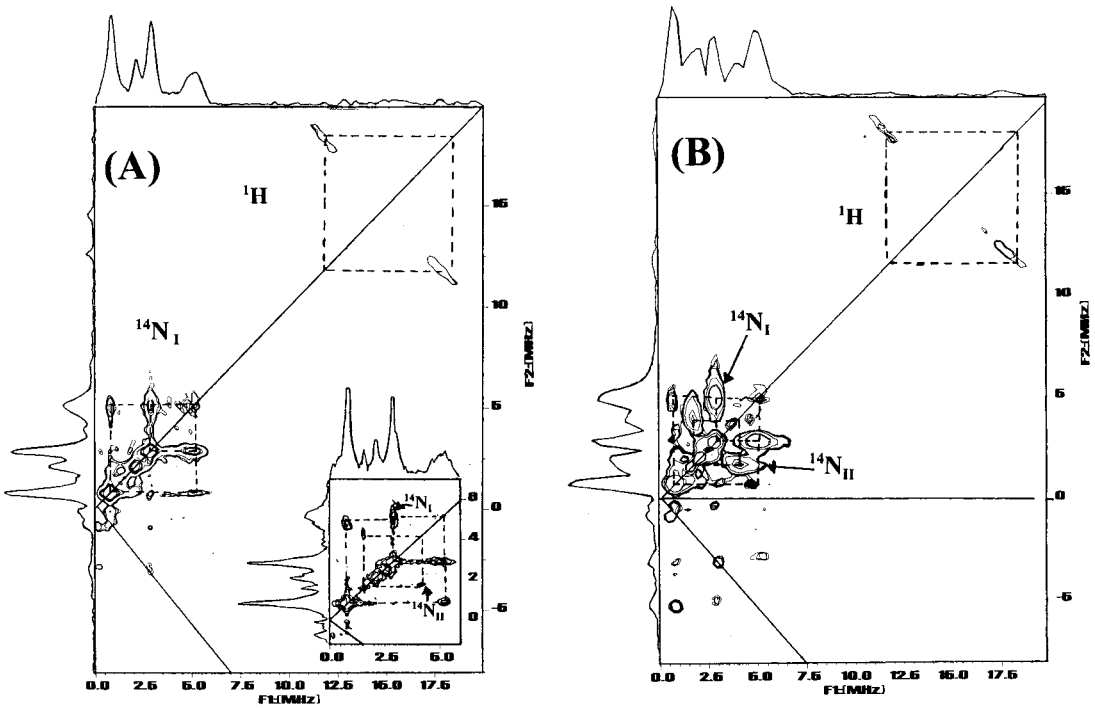

Figure 3. Contour plots of 2D-HYSCORE spectra for Q_A^- in CN-treated PSII buffered at pH = 9.2 (panel A), pH = 8.3 (inset in panel A), or pH = 6.3 (panel B). Experimental conditions: H = 3458 G; sample temperature, 16 K; τ = 128ns; and other conditions as in Figure 2.

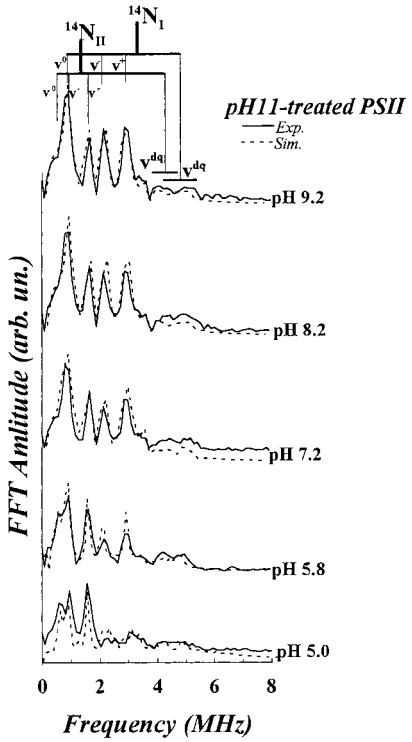

Figure 4. Fourier transform of the 3-pulse ESEEM recorded for Q_A^- in pH 11-treated PSII buffered at the indicated pH values (solid lines). The simulated spectra (dashed lines) have been calculated by using the coupling parameters listed in Table 1B. The various features are labeled according to their origin. Experimental conditions: H = 3457 G; sample temperature, 18 K; τ = 104 ns; time interval between successive pulse sets, 3 ms; and microwave frequency, 9.64 GHz.

spectra (see Figure 4) are similar to those reported earlier[10] for comparable PSII samples.

It is of relevance to note the similarity between the ESEEM spectra for CN-treated PSII at pH < 7.2 (Figure 2) and pH 11-treated PSII at pH > 5.8 (Figure 4). This shows that, in these two quite different PSII preparations, the environment of Q_A^- is comparable when compared at appropriate values of pH. Taking into account the analysis for the spectra in Figure 2 (see also the numerical simulations of the ESEEM spectra in ref 10), the features at 0.8, 2.1, and 2.88 MHz are due to the N_I coupling to Q_A^-, while the feature at 1.7 MHz together with part of the features at 0.5−0.8 MHz is due to N_{II} coupling to Q_A^-. This shows that, at pH values above 5.8, Q_A^- is coupled to both the N_I and N_{II}.

At pH 5.8, the features due to N_I (at 2.1 and 2.85 MHz) are weaker than the feature at 1.7 MHz due to N_{II}. At lower pH values these intensity differences become more prominent (see Figure 4): at pH 5.0 the features due to N_{II} clearly dominate the spectrum; that is, the peaks at 1.54, 0.95, and 0.65 MHz become more prominent, while the features due to N_I are hardly resolved. These spectral changes are reversible: when the pH 5.0 sample was washed and resuspended at pH 9.2, its ESEEM spectrum (not shown) became virtually identical to that shown in Figure 4 for the sample at pH 9.2.

The HYSCORE spectra for the Q_A^- in pH 11-treated PSII at pH 9.2 or 5.0 are displayed in Figure 5, parts A and B, respectively.

The spectrum in Figure 5A is comparable to the HYSCORE spectrum in Figure 3B: the ridges centered at (1.5 MHz, 4.3 MHz) and (0.9 MHz, 4.3 MHz) correspond to the (ν_+, ν_{dq}) and (ν_0, ν_{dq}) crosspeaks, respectively, due to the N_{II} coupling. The strong crosspeaks (ν_+, ν_{dq}) centered at (2.8 MHz, 5.1 MHz) are due to N_I coupling. The spectrum at pH 5.0, Figure 5B, contains crosspeaks due to both N_I and N_{II} coupling. Noticeably, the (ν_+, ν_{dq}) features of N_I at frequencies (2.9 MHz, 5.1−6.4 MHz) attain a characteristic elongated shape, and this indicates that the N_I coupling is characterized by significant hyperfine anisotropy.

Thus the HYSCORE spectrum in Figure 5B shows that at pH 5.0 *both* N_I and N_{II} are coupled to the Q_A^-. The N_I coupling

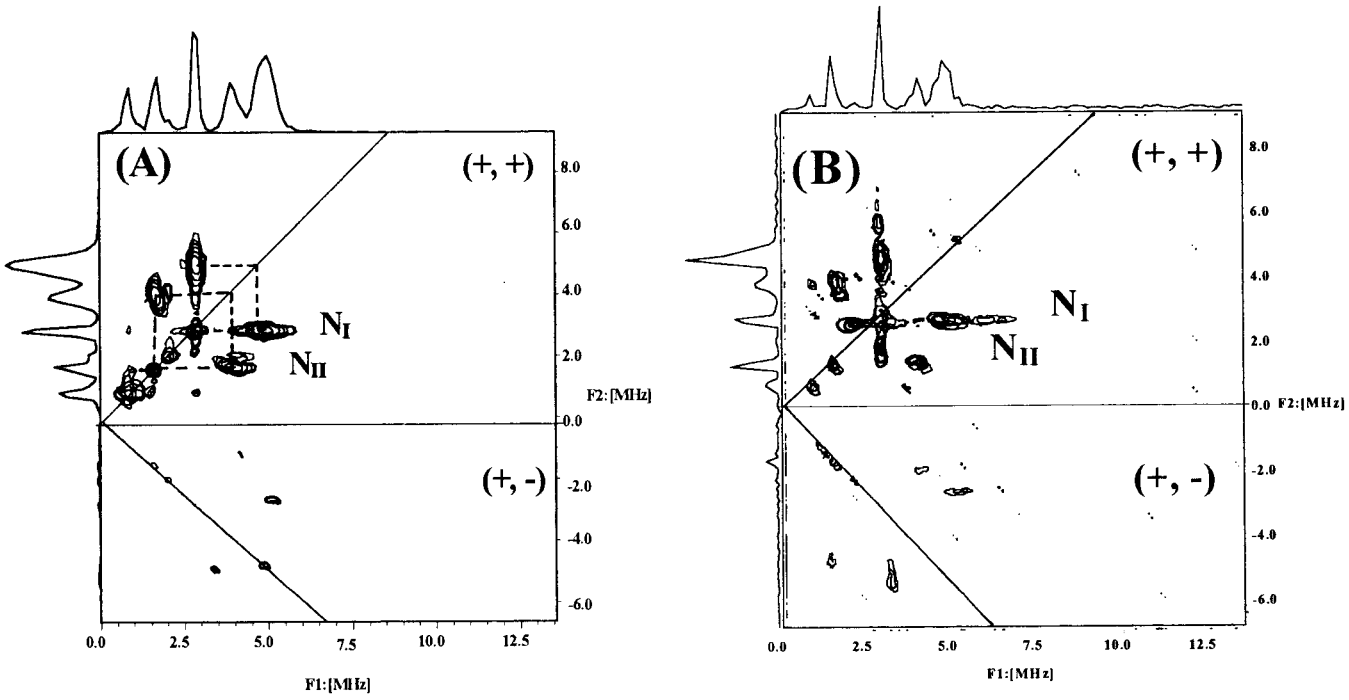

Figure 5. Contour plots of 2D-HYSCORE spectra for Q_A^- in pH 11-treated PSII buffered at pH = 9.2 (A) and pH 5.0 (B). Experimental conditions: $H = 3457$ G; sample temperature, 16 K; $\tau = 160$ ns; and other conditions as in Figure 2.

is characterized by strong hyperfine anisotropy, and this is the reason for the degradation of the features from N_I at pH 5.0 in Figure 4.

In summarizing, the present results show that pH affects the ^{14}N couplings to Q_A^- in both CN-treated PSII and pH 11-treated PSII. The HYSCORE spectra allow the assignments of the observed nuclear frequencies for N_I, N_{II}, and ^1H nuclei and estimation of their coupling parameters. This approach, in combination with numerical simulations (presented below), allows a more accurate estimation of the coupling parameters.

Simulations of the ^{14}N-ESEEM. Numerical simulations of the ESEEM spectra were performed by assuming that the low-frequency features arise from two ^{14}N nuclei, according to the HYSCORE data. The ^1H coupling, which is resolved in HYSCORE spectra, has no resolvable influence on the simulated 1D-ESEEM spectra (not shown); thus, to simplify the discussion, the ^1H couplings are not included in the simulations. In this context, the simulation was focused on (a) the reproduction of the frequency positions of the basic ^{14}N features and (b) the variation of the relative intensities of the two ESEEM subspectra, that is, due to N_I and N_{II} as it is observed for various pH values. The simulated ESEEM spectra are displayed in Figures 2 and 4 (dashed lines). The weak features at ~3.1 MHz and ~4.2 MHz resolved in some of the simulated spectra are "combination lines", that is, of the $\upsilon^-(N_I) + \upsilon^-(N_{II})$ and $\upsilon^+(N_I) + \upsilon^+(N_{II})$ frequencies, respectively; these are due to the simultaneous coupling of both N_I and N_{II} to the electron spin (see also refs 10 and 22). The coupling parameters used in the simulations are listed in Table 1. In all spectra, the Euler angle β has a definite influence on the relative intensities of the υ^0, υ^-, and υ^+ features. The angles α, γ have no resolvable influence on the calculated spectra and are set equal to zero.

Q_A^- in CN-Treated PSII. The ESEEM spectra of Q_A^- in CN-treated PSII (Figure 2) were simulated by using an almost pH-independent set of coupling parameters for $^{14}N_I$ plus a strongly pH-dependent hyperfine coupling tensor for $^{14}N_{II}$ (see Table 1A). As seen from Table 1A, in CN-treated PSII, the A_{iso} of N_I is always close to the cancellation condition (A_{iso} = 2.1 MHz), and consequently, the corresponding ESEEM features remain intense and sharp[34] throughout the pH range studied. As a result, the coupling parameters for N_I are determined with a high accuracy from the experimental frequency domain spectra. On the other hand the weakening of the A_{iso} for N_{II} at alkaline pH leads to a diminution of its ESEEM spectrum;

Table 1. A ^{14}N hyperfine (A_x, A_y, A_z) and nuclear quadruple parameters (e^2qQ_n/h, η) for Q_A^- in CN-Treated PSII and pH 11-Treated PSII

	$^{14}N_I$			$^{14}N_{II}$		
pH	(A_x, A_y, A_z)[a] (MHz)	e^2qQ_n/h (MHz)	η	(A_x, A_y, A_z)[a] (MHz)	e^2qQ_n/h (MHz)	η
	(A) CN-Treated PSII					
5.5	(2.0, 1.7, 2.8)	3.25	0.45	(1.5, 1.5, 2.3)	1.56	0.77
	± 0.1	± 0.05	± 0.02	± 0.1	± 0.05	± 0.05
5.8	(2.0, 1.7, 2.8)	3.25	0.45	(1.5, 1.5, 2.3)	1.56	0.77
	± 0.1	± 0.05	± 0.02	± 0.1	± 0.05	± 0.05
6.3	(2.0, 1.7, 2.8)	3.25	0.45	(1.3,1.3,2.1)	1.56	0.77
	± 0.1	± 0.05	± 0.02	± 0.1	± 0.05	± 0.05
7.2	(2.0, 1.7, 2.6)	3.25	0.45	(1.2, 1.2, 2.0)	1.65	0.75
	± 0.1	± 0.05	± 0.02	± 0.1	± 0.10	± 0.10
8.2	(2.0, 1.7, 2.6)	3.25	0.45	(1.1, 1.1, 1.9)	1.65	0.75
	± 0.1	± 0.05	± 0.02	± 0.1	± 0.10	± 0.10
9.2	(2.0, 1.7, 2.6)	3.25	0.45	(0.2, 0.2, 0.9)	1.65	0.75
	± 0.1	± 0.05	± 0.02	± 0.3	± 0.20	± 0.20
	(α, β, γ) = (0°, 40°, 0°) ± 10°			(α, β, γ) = (0°, 50°, 0°) ± 10°		
	(B) pH 11-Treated PSII					
5.0	(1.3, 1.3, 3.7)	3.25	0.45	(1.5, 1.5, 2.6)	1.47	0.78
	± 0.1	± 0.05	± 0.05	± 0.1	± 0.03	± 0.02
5.5	(1.4, 1.4, 3.6)	3.25	0.45	(1.5, 1.5, 2.6)	1.47	0.78
	±0.1	± 0.05	± 0.05	± 0.1	± 0.03	± 0.02
5.8	(1.6, 1.6, 3.2)	3.25	0.45	(1.4, 1.2, 2.4)	1.52	0.77
	±0.1	± 0.05	± 0.02	± 0.1	± 0.03	± 0.03
7.2	(1.7, 1.7, 2.9)	3.25	0.45	(1.4, 1.3, 2.2)	1.58	0.77
	±0.1	± 0.05	± 0.02	± 0.1	± 0.03	± 0.05
8.2	(2.0, 1.7, 2.6)	3.25	0.45	(1.4, 1.4, 2.2)	1.58	0.71
	± 0.1	± 0.05	± 0.02	± 0.1	± 0.05	± 0.02
9.2	(2.0, 1.7, 2.8)	3.25	0.45	(1.4, 1.4, 2.2)	1.58	0.71
	± 0.1	± 0.05	± 0.02	± 0.1	± 0.05	± 0.02
	(α, β, γ) = (0°, 40°, 0°) ± 10°			(α, β, γ) = (0°, 50°, 0°) ± 10°		

[a] The indicated error margins refer to A_{iso} values; the errors for the anisotropic components are represented by the error bars in Figure 6.

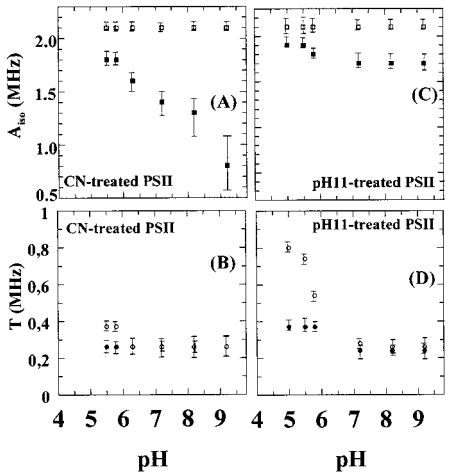

Figure 6. Plot of the experimental hyperfine coupling parameters vs pH, for the ^{14}N couplings to Q_A^- in PSII: A_{iso} vs pH plot for CN-treated (panel A) and pH-11-treated PSII (panel C) and T vs pH plot for CN-treated (panel B) and pH-11-treated PSII (panel D). The couplings are calculated as $A_{iso} = (A_x + A_y + A_z)/3$, $T = (A_{iso} - {}^1/_2(A_x + A_y))/2$ with the $A_{x,y,z}$ values taken from Table 1: open symbols (□, ○), N_I couplings; and solid symbols (■, ●), N_{II} couplings.

consequently, at alkaline pH only upper limits in the hyperfine coupling of N_{II} in CN-treated PSII can be determined (Table 1A).

According to the preceding analysis of the ESEEM data in CN-treated PSII, the observed variations in the ESEEM spectra as a function of the pH (Figure 2) are interpreted as due to a progressive weakening of the N_{II} hyperfine coupling, while the population of the coupled N_{II} nuclei is kept constant. An alternative explanation for this effect is that it results from a decrease of the population of N_{II} nuclei coupled to Q_A^- spin, rather than a weakening in the A_{iso} itself. To test this possibility, the total ESEEM spectrum at all pH values studied was simulated by combining simulated ESEEM spectra of N_I and N_{II}, obtained for the spectrum at pH 5.0 (i.e., where the N_{II} is strongest), and by decreasing the contribution from the N_{II} spectrum while maintaining A_{iso} constant. A plot of the population where N_{II} is coupled to the Q_A^- spin vs pH (not shown) reveals the same qualitative trend as the variation of $A_{iso}(N_{II})$ vs pH, shown in Figure 6A: in CN-treated PSII at pH 6.3, or lower, all of the N_{II} nuclei are coupled to the Q_A^- spin, while at pH > 8.3 the coupling of N_{II} is severely weakened or even absent. In summary, both mechanisms, that is, weakening of A_{iso} and/or some N_{II} population decrease, are possible but only at pH > 7.2. This uncertainty is reflected in the increasing error bars in the A_{iso} values of N_{II} at pH > 7.2. On the other hand, at pH ≤ 7.2 the shifts of the average υ_{dq} frequency N_{II}, which can be resolved in the HYSCORE spectra, clearly show that a progressive weakening of the A_{iso} takes place as a function of the pH, and this can fully account for the observed changes in the ESEEM spectra at pH ≤ 7.2. Astashkin et al.[22] showed that in CN-treated PSII at pH 7.5 the features of N_{II} are weakened due to a low A_{iso} which deviates from the cancellation condition. Although the role of pH that we show here has been overlooked by these authors, they clearly show that their data are convincingly explained by only decreasing A_{iso}, keeping the N_{II} population constant. Overall it is clear that the mechanism involving the weakening of the A_{iso} of N_{II} as the pH is increased is the more straightforward explanation for the effects observed.

Q_A^- in pH-11-Treated PSII. The experimental spectra ESEEM spectra of Q_A^- in pH 11-treated PSII (Figure 4) have been simulated by using hyperfine tensors with strongly pH-dependent anisotropy for $^{14}N_I$, the A_{iso} being almost pH-independent (see Table 1B). In contrast, the hyperfine coupling parameters for $^{14}N_{II}$ are less dependent on the pH (see Table 1B).

In Figure 6, we display plots of the various hyperfine coupling parameters, taken from Table 1, as a function of the pH.

According to these plots, it is important to underline the two distinct effects of pH on the N_I and N_{II} couplings: in CN-treated PSII (Figure 2) the features due to N_{II} coupling become weak at alkaline pH due to a *decrease* of the A_{iso} of N_{II}. In Figure 4, that is, in pH 11-treated PSII, the features due to N_I coupling degrade but this is due to a strengthening of the coupling, that is, *increasing hyperfine anisotropy*.

Discussion

Before discussing the implications of the specific findings concerning the pH effects described in this work, we shall discuss the origin of the couplings detected and provide arguments that these couplings are mediated by hydrogen bonds.

Assignment of the Interacting ^{14}N. It has been amply demonstrated that the electron acceptor side of PSII is closely structurally related to that of bacterial reaction centers.[21] The similarities between the two types of reaction centers extend to the two classes of nitrogen couplings to Q_A^-, which are detected by ESEEM[10,13−16]. The NQI parameters in Table 1, when compared to previous NQI[35] and ESEEM data,[10,13−16] support the assignment of the detected ^{14}N couplings to Q_A^- to a peptide (N_I) and an amino imidazole Nδ- nitrogen (N_{II}). These assignments are firmer in PSII[23c] but are very likely to be correct in bacterial reaction centers also since X-ray crystallographic models [21c] have shown that Q_A is likely to be H-bonded to a peptide amide nitrogen and an imidazole Nδ-H group. Experimental evidence for H-bonds to bacterial Q_A^- has been obtained from ENDOR[20] and FTIR[36] data. Overall it seems highly likely that the H-bonding situation in PSII is comparable to that in the bacterial reaction center and that the nitrogen couplings are mediated through the H-bonds. The basis for the physical mechanism for such couplings is described below.

The Role of H-Bonds. The existence of nonzero A_{iso} for the interacting ^{14}N nuclei indicates that a nonzero electron spin density is transferred from the Q_A^- onto these ^{14}N nuclei. In all reported cases in the literature[10,13−16] as well as in the current work, A_{iso} values of around 1−2 MHz have been reported for the ^{14}N couplings to Q_A^-, and this corresponds to *s*-spin densities

(35) Hunt M. J.; Mackay, A. L. *J. Magn. Res.* **1976**, *22*, 295. (b) Edmonds, D. T. *Phys. Rev. C: Nucl. Phys.* **1977**, *29*, 233. (c) Ashby, C. H.; Paron W. F.; Brown, T. L. *J. Am. Chem. Soc.* **1980**, *102*, 2290.

(36) Breton, J.; Bourie, J.; Boullais, R.; Berger, C. G.; Nabedryk, E. B*iochemistry* **1994**, *33*, 12405. (b) Brudler, R.; de Groot, H. J. M.; van Liemt, W. B. S.; Steggerda, W. F.; Esmeijer, R.; Gast, P.; Hoff, A. J.; Lugtenbourg J.; Gerwert, K. *EMBO J.* **1994**, *13*, 5523.(c) After submission of this paper, two reports appeared on the characterisation of the Q_A^- environment by FTRIR.[36d,e] In ref 36d the authors used PSII labeled with ^{15}N-His to argue that a hydrogen bond exists between Q_A and an imidazole nitrogen in accordance with the earlier ESEEM work and the present article. In ref 36e the authors had performed FTIR on a series of different biochemical preparations of PSII in which the iron was perturbed or removed. The FTIR results verified the earlier conclusion,[14] which is corroborated by our present data, that in CN-treated PSII at pH 8 the H-bond between Q_A^- and the interacting His is severely weakened. That paper raised the problem that some of the preparations led to loss of H-bonding between Q_A and the protein residues.[36e] Their data were obtained using samples where each was at a different pH value, a fact that is overlooked in this FTIR work. Given the present findings, some of their conclusions that were based on comparison of FTIR spectra for Q_A^- in different types of PSII preparations may have to be reconsidered by comparing samples at the appropriate pH values. (d) Noguchi, T.; Inoue, Y.; Tang, X.-T. *Biochemistry* **1999**, *38*, 399. (e) Noguchi, T.; Kurreck, J., Inoue, Y.; Renger, G. *Biochemistry* **1999**, *38*, 4846.

of the order of ~0.1−0.2% at the ^{14}N nuclei.[37] This extent of transferred spin density has been previously observed at ^{13}C and ^{14}N nuclei H-bonded to either nitroxide or aliphatic radicals.[38a−f] In both cases, NMR data together with MO calculations[38a−f] on the interaction between open and closed shell systems, that is, the radical and the ^{14}N-bearing moiety, showed that the H-bonded proton forms part of the spin transfer pathway from the radical to the hydrogen-bonded atom.

According to this earlier work[38a−f] there are two mechanisms responsible for the spin transfer: first, spin polarization, which results in a *negative* s-spin density transferred at the proton while *positive* s-spin density is transferred onto the next atom, that is, the nitrogen; and, second, direct spin delocalization from the π-electron spin of the Q_A^- ,which puts *positive* spin density on both the ^{1}H and the ^{14}N nucleus. Consequently, the spin density on the H nucleus might become negligibly small due to mutual cancellation, while the additive character of the spin densities on the ^{14}N results in a nonzero spin density.

This model is applicable to the case of Q_A^- hydrogen-bonded to the protein in the photosynthetic reaction center. In particular, it fits nicely with the findings from ^{1}H-ENDOR data on the Q_A^-, which measure purely dipolar **A** tensors with almost zero A_{iso} values for the (N)-H protons,[19,20] while ESEEM data show that nonzero spin density is transferred to the H-bonded nitrogens.[10,13−16] More recent hybrid density-functional calculations for an imidazole H-bonded to a phenol radical corroborate this view, showing that spin polarization through the H-bonded proton transfers spin density to the interacting N nucleus.[38g] Analogous theoretical calculations for the Q_A^- in PSII and bacteria, like those recently published for a plastoquinone radical H-bonded to alcohol solvent,[38h] should allow a quantitative analysis of the role of the H-bonds in the spin-transfer mechanism.

Previous ESEEM[39a] and nuclear quadrupole resonance[39b] work for imidazole ^{14}Nδ nuclei showed that the parameters e^2qQ_n/h and η are sensitive to hydrogen-bonding effects.[39] According to the Towens-Dailey model[40] the electron occupancy of the lone-pair orbital of Nδ is sensitive to the H-bonding effects, and this is reflected in the e^2qQ_n/h and η values. According to this, it is expected that a strong H-bond would lower the ^{14}N lone-pair population with a subsequent reduction of the e^2qQ_n/h value and a concomitant increase of η.[39a] In Figure 7 we present a plot of h/e^2qQ_n versus the asymmetry parameter η for the observed ^{14}Nδ couplings in PSII, from Table 1.

This plot visualizes *trends* related to the NQI values, that is, in such a h/e^2qQ_n vs η plot a shift toward the origin of the axes reflects a relative weakening of the H-bond of the Nδ (for a complete analysis see ref 39a,b). For comparison, we have included in the same plot the NQI values reported for histidine ^{14}Nδ interacting with the Q_A^- [15,16] and Q_B^-[16] in bacterial reaction centers.

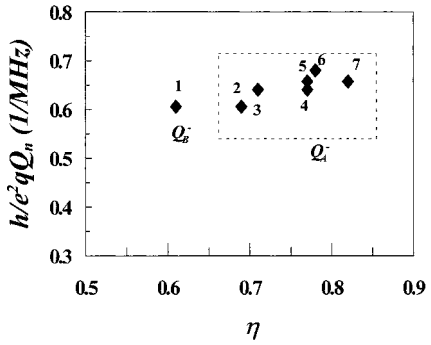

Figure 7. Plot of the experimental h/e^2qQ_n vs η values of the experimental ^{14}N$\delta^{(1)}$ couplings to semiquinones in PSII and bacterial reaction centers: (1) Q_B^- in *Rhodobacter sphaeroides* (ref 16); (2) Q_A^- in *Rhodopseudomonas viridis* (ref 16); (3) Q_A^- in high pH-treated PSII pH 9.2 (this work); (4) Q_A^- in CN-treated PSII, pH 5.5 (this work); (5) Q_A^- in LiClO[4]-treated PSII pH 6.0 (ref 22); (6) Q_A^- in high pH-treated PSII pH 5.0 (this work); and (7) Q_A^- in *Rhodobacter sphaeroides R26* (ref 15).

Despite some scattering, we see that, in PSII and bacteria, the points in Figure 7 cluster in a region corresponding to relatively low values of e^2qQ_n/h and high values of η. According to the Towens-Dailey[40] model, this indicates a relatively low degree of occupancy of the lone-pair orbital of the Nδ and may be correlated with the presence of H-bonds.[39a] In Figure 7, the point corresponding to the Nδ interacting with Q_B^- in *R. sphaeroides* falls closer to the origin of the axes, and this is consistent with the idea that Q_B^- forms weaker H-bonds than Q_A^-. In the same plot, the points for the Nδ coupling in CN-treated PSII at various pH's are located close to that of the Nδ interacting with Q_A^- in *R. sphaeroides*. In pH 11-treated PSII at pH 5.0, where the Nδ coupling appears to be best resolved among all cases, the NQI parameters clearly indicate a significant H-bond strength.

Having established that the nitrogen couplings to Q_A^- are very likely mediated by H-bonding, we shall now discuss the observed pH effects, their relationship to previous reports, and their structural significance. In CN-treated PSII, ESEEM and HYSCORE data reported here show that, at acidic pH values, the Q_A^- radical is magnetically coupled with two ^{14}N protein, a backbone nitrogen (N_I), and the amino nitrogen, Nδ, of an imidazole (N_{II}). A specific effect of pH on the protein environment of Q_A^- occurs, that is, a weakening of the magnetic coupling of Nδ with Q_A^- as the pH is increased so that at pH values higher than pH 8.2 the Nδ is not detectable. In clear contrast, the coupling of Q_A^- with N_I is pH-independent.

In the high pH-treated sample, both nitrogen couplings are present at all pH values; however at pH < 5.8 the Nδ coupling dominates the ESEEM spectrum. The intensity of the spectral features due to N_I is diminished due to an increase in the anisotropic part of the hyperfine coupling (see Figure 4). The anisotropic part of the hyperfine coupling A_{aniso} consists of two contributions,[41] $A_{aniso} = A_{dip} + A_p$. In this equation A_{dip} is the dipolar interaction between the ^{14}N nucleus and the Q_A^-. In the point-dipole approximation, this is given by the relation $A_{dip} = \Sigma\, \rho_i g_e g_n \beta_e \beta_n / (R_i)^3$, where ρ_i is the unpaired spin density at the ith atom of the Q_A^-, R_i is the distance of the ^{14}N nucleus from the ith atom, g_e is the electron g factor, $g_{n\ is}$ the nuclear g-factor, and β_e and β_n are the electron and nuclear Bohr magnetons, respectively. The most significant fraction (~0.2−0.3) of the electron spin density in semiquinones is localized

(37) Morton, J. R.; Preston, K. F. *J. Magn. Res.* **1978**, *30*, 577.
(38) Morishima, I.; Endo, K.; Yonezawa, T. *J. Chem. Phys.* **1973**, *58*, 3146. (b) Morishima, I.; Inubushi, T.; Endo, K.; Yonezawa, T.; Goto, K. *J. Am. Chem. Soc.* **1972**, *94*, 4812. (b) Kabankin, A. S.; Zhidomirov, G. M.; Buchachenco, A. L. *J. Struct. Chem.* **1972**, *13*, 423. (c) Morishima, I.; Endo, K.; Yonezawa, T. *Chem. Phys. Lett.* **1971**, *9*, 143. (d) Morishima, I.; Endo, K.; Yonezawa, T. *J. Am. Chem. Soc.* **1971**, *93*, 2048. (e) Morishima, I.; Toyoda, K.; Yoshikawa, K.; Yonezawa, T. *J. Am. Chem. Soc.* **1973**, *95*, 8627. (f) Morishima, I.; Inubushi, T., K.; Yonezawa, T. *J. Am. Chem. Soc.* **1976**, *98*, 3806. (g) O'Malley, P. O. *J. Am. Chem. Soc.* **1998**, *120*, 5093. (h) O'Malley, P. O. *J. Am. Chem. Soc.* **1998**, *120*, 11732.
(39) Jiang, F.; McCracken J.; Peisach J. *J. Am. Chem. Soc.* **1990**, *112*, 9035. (b) Hiesh, Y. N.; Rubenacker, G. V.; Cheng, C. P.; Brown T. L. *J. Am. Chem. Soc*. **1977**, *99*, 1384.
(40) Townes, C. H.; Dailey, B. P. *J. Chem. Phys.* **1949**, *17*, 782.
(41) Gordy, W. *Theory and Applications of Electron Spin Resonance*; John Wiley & Sons: New York, 1980; pp 198−304.

on the keto groups.[19−20] Thus we consider that the major part of A_{dip} refers to the distance between the keto group of Q_A^- and the interacting ^{14}N nucleus (see also discussion in ref 14). The second part, A_p, is the anisotropic hyperfine interaction due to *p*-electron density at the ^{14}N nucleus. A *p*-orbital with unpaired spin-density ρ_p, would result in $A_p = C\rho_p$, where the proportionality constant C is ∼55 MHz.[37] According to the present data, Tables 1, in high pH-treated PSII, a ∼3-fold increase of the A_{aniso} of N_I is observed on going from pH 5.0 to pH 9.2. If this was exclusively due to an increase of the A_{dip}, then this would correspond to shortening of the Q_A^-−N_I distance by a factor of $\sim(3)^{1/3}$ ∼1.44. In the other limit, the increase of the A_{aniso} of N_I by ∼ 0.6 MHz is exclusively due to an increase of A_p: in such a case, the A_p of 0.6 MHz would correspond to an increase of ρ_p by 0.6/55 ∼ 1%.[37] A significant ρ_p spin density at the nitrogen might result in nonaxial A_p tensor which in the case of nonlinear NH···O arrangement would result in a nonaxial *A* tensor; the hyperfine tensors given in Table 1B, however, are axial but this most likely is due to limited resolution.

In summary, a pure dipolar effect would require a rather significant shortening of the Q_A^-−N_I distance, that is, by a factor of ∼1.44. On the other hand, a small change of the ρ_p spin density by ∼1% would suffice to cause the observed increase of the A_{aniso} of N_I. Given the specificity and the reversibility of the observed pH effects, we consider a Q_A^-−N_I distance change by a factor 1.44 to be unrealistically large. A more reasonable explanation is a small compression of the Q_A^-−N_I distance at acidic pH, resulting in a small increase of both A_{dip} and the transferred ρ_p spin-density on N_I due to a more efficient overlap between the orbitals of Q_A^- and those of N_I.

Relation to Published Results. The present results provide an explanation for some apparently contradictory reports in the literature concerning the interactions between the Q_A^- and protein nitrogen nuclei: In our original paper[14] we found that, in CN-treated PSII at pH 8, the ESEEM of Q_A^- is due to the coupling to a single backbone nitrogen (N_I). However, Astashkin et al.[22] recently reported that, in addition to N_I, modulations due to N_{II} are also detected by ESEEM of Q_A^- in CN-treated PSII. These results can now be reconciled in terms of the pH dependence of the N_{II} coupling in CN-treated PSII: in ref 22 samples were buffered at pH 7.5, while in ref 14 samples were at pH 8.1.[42] Here we show that, at pH 7.5, the N_{II} coupling results in a weak but resolvable contribution to the ESEEM spectrum, while at pH 8.1 the N_{II} coupling is small and is hardly resolvable (see Figure 2). However, we should note that, even at pH 7.5, the N_{II} coupling deviates significantly from the cancellation condition, and due to this, its contribution to the ESEEM spectrum is obscured by the N_I features. Thus the analysis of N_{II} coupling made in ref 22, although detailed, was based on a nonoptimal ESEEM spectrum where the N_{II} contribution is small. In contrast, as is shown by the data in Figure 2, a pH value of <6.3 would result in maximal contribution of both ^{14}N couplings.

In ref 23a, a pH effect on the N_{II} coupling in CN-treated PSII from *Synechosystis* was reported. This observation is in qualitative agreement with the present results of the pH effect in CN-treated in plant PSII. However, at the higher of the two pH values shown in ref 23a (pH 9.2), the N_{II} feature is small but still clearly detectable, while in the present study the N_{II} is not detectable at pH 9.2. This could represent either a species difference or a difference in the biochemical procedures used.[42]

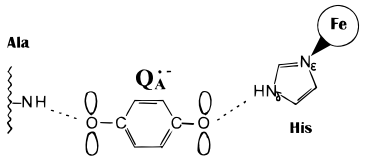

Figure 8. A working model of the Q_A^- environment in PSII.

Structural Implications. The present ESEEM and HYSCORE data provide some structural information which help one to understand the nature of the changes occurring in the Q_A^- site upon changing the pH. For the CN-treated system, decreasing the pH leads to the strengthening of the Q_A^- coupling to the imidazole Nδ nitrogen. The following observations can be made concerning the nature of this change.

(1) No significant change occurs to the N_I coupling (see Figure 6), indicating practically no change in the structural relationship between the semiquinone the peptide nitrogen.

(2) No change in the orientation of the quinone ring relative to the protein occurs. This is deduced from the finding that the orientation of the tensor **Q** vs **A** is unchanged (see Table 1A). In previous ESEEM[39a] and NQR[39b,43] work, it was demonstrated that the orientation of q_{zz} axis of the **Q** tensor depends on the size of the quadrupole coupling parameters. Thus the NQI parameters for the N_{II} coupling listed in Table 1A imply that the q_{zz} axis is perpendicular to the imidazole ring plane. The finding that the orientation of the tensor **Q** vs **A** remains the same at all pH values indicates that the change occurring with pH does not involve rotations of the His or the amide group relative to the quinone ring.

(3) The spin density on the semiquinone is not altered significantly by the pH change. This is judged from the ^1H couplings. The ^1H coupling of $A_{iso} \sim 5.7$ MHz, which is resolved in the HYSCORE spectra, is due to protons either of the semiquinone ring or from its protein environment. Based on published ^1H-ENDOR[19,20] data on Q_A^-, this almost purely isotropic coupling is assigned to ring protons of the Q_A^-. Within the resolution of our data, this ^1H coupling is unaffected by the pH, and this indicates that the spin density on Q_A^- does not undergo significant changes upon changing the pH.

Overall, the present data indicate that the pH effect in CN-treated PSII is quite specific and reversible, involving a change in the imidazole relative to the semiquinone/peptide. In the high pH-treated PSII, lowering the pH strengthens the existing coupling between the imidazole and the semiquinone, resulting in the so-called "fingerprint" ESEEM spectrum of an imidazole coupling (see Figure 4, pH 5.0). In this case, the coupling to the peptide is also affected, becoming more anisotropic. For the reasons discussed above, we consider that this is most likely due to a small compression of the Q_A^- −N_I distance.

In the following, on the basis of the plots in Figure 6, we attempt to rationalize the pH data in the two kinds of biological sample. In the CN^--treated sample, the nonheme iron remains in the site.[12] On the basis of the structure of the bacterial reaction center, it is assumed that the iron is coordinated to the Nϵ of the imidazole, whose Nδ H-bonds to the semiquinone carbonyl (see Figure 8).

(42) In our original article on the ESEEM of Q_A^- in CN-treated PSII,[14] we reported that changing the pH from 8.1 to 6.0 had little effect on the spectra. This appears to contradict the present findings. We have found that washing (i.e., dilution and pelleting) of the sample and incubation for 40 min in the appropriate buffer seems to be required for the pH effects to be fully induced. When samples were simply pelleted, washed free of their treatment buffer, and resuspended up to sample volume in the buffer of the required pH, then the changes described above were much less marked. Our earlier report[14] probably reflects the fact that the pH was adjusted in the sample tube.

(43) Lucken, W. A. C. *Nuclear Quadrupole Coupling Constants*; Academic: London, U.K., 1969.

According to Figure 6 the A_{iso} coupling for Nδ undergoes a steep decrease between pH 7−8. This pH effect may arise from an amino acid residue which has a pK in the region of pH 7.5. Above the pK the H-bond to the imidazole is weak or absent. Below the pK, a change occurs in the protein, which results in a strengthening (or formation) of the H-bond from the imidazole to the Q_A^-. The H-bond to the peptide on the semiquinone carbonyl distal to the iron is unaffected. Thus, a more acidic pH could result in a decrease in the distance between the Fe/imidazole and the semiquinone/peptide. This model is corroborated by FTIR data in CN-treated PSII at alkaline pH 8,[36c] which report a severe weakening of the H-bond in this sample, overlooking, however, that this is due to pH.

In the high pH-treated sample, we consider that the nonheme iron is absent (see 11c). In iron-depleted PSII, the imidazole involved in H-bonding to the semiquinone is unattached at its imino nitrogen. This imidazole then is no longer restrained by its attachment to the iron, and thus, it is free to be relatively strongly H-bonded to the semiquinone throughout the pH range studied. At low pH values, a strengthening of this coupling does, however, occur (see Figure 6). This may again reflect a pH-dependent conformational change in the site, resulting in a slight compression of the site and hence stronger H-bonding.

The identity of the amino acid group undergoing ionization upon changing the pH is a matter for speculation. The involvement of the H-bonding amino group of the imidazole itself is ruled out, at least in the case where the iron is absent, where the Nδ coupling, and thus, the H-bond is always present irrespective of the pH.

It seems worth considering a model in which the two different pK_a values occurring in the two different kinds of material (with iron present in CN-treated and iron absent in pH 11-treated PSII) reflect the same amino acid. If so, the higher pK_a in CN^--treated PSII may be rationalized by the fact that the region close to the iron in this material is likely to experience a higher negative charge since at least two CN^- ions are thought to be bound.[12]

Extrapolating from this model to the untreated PSII reaction center, we would predict a H-bonding pattern like that in the CN^--treated sample since the iron is of course present (see Figure 8). However, in the absence of the cyanide, the pK_a of the group modulating the structure of the site would be predicted to be at a pH lower than that seen for cyanide. A pH effect on the EPR signal of semiquinone−iron $Q_A^-Fe^{2+}(S = 2)$ has been reported.[3] At high pH the so-called $g = 1.9$ form is seen, while at low pH the $g = 1.82$ form is seen.[3,47c] The strengthening of the H-bonding from Q_A^- to the imidazole/iron at low pH is consistent with the idea that the $g = 1.82$ form, seen at low pH, being more shifted from the $g = 2$ value of the semiquinone, represents a more strongly coupled system

The existence of an ionizable amino acid residue determining the magnetic interaction between the semiquinone and the iron was evidenced by experiments where the labile physiological ligand of the iron, bicarbonate, was replaced by various carboxylate anions.[47a,b] It was shown that the carboxylate ligand to the iron influences the pK_a of the ionizable amino acid residue that in turn determines the g value for $Q_A^-Fe^{2+}(S = 2)$ and the redox potential of the iron.[47a] It is possible that this ionizable amino acid plays a role in the pH effects detected by ESEEM.

This model, that is, the interacting histidine forming part of the spin-exchange pathway between the nonheme iron and Q_A^- in PSII, is corroborated by EPR data in *R. sphaeroides*, where the nonheme iron has been replaced by Cu^{2+}. In this work,[44,45] the study of the magnetic interaction between the metal and the semiquinone in ^{14}N- and ^{15}N-labeled reaction centers showed that the exchange interaction between the metal and the semiquinone involves M-His219 and the H-bond of its Nδ to Q_A^-. On the basis of the similarity of the exchange interactions in Fe^{2+}-containing, that is, native, and Cu^{2+}-containing reaction centers, it was suggested that the histidine plays a similar role in the native reaction centers.[45]

Finally it is worth pointing out that the pH-induced structural changes discussed here could have functional significance with regard to the regulation of electron transfer in PSII. It has been recently demonstrated that the E_m of Q_A/Q_A^- is modulated by distant structural changes (e.g., binding of Ca^{2+}),[46] and it has been postulated that variations in the E_m of Q_A/Q_A^- determine the back reaction pathway and hence the susceptibility of PSII to photodamage.[46c] The pH effects reported here provide a range of specific factors which could be important in the modulation of the E_m of Q_A/Q_A^-: the H-bonding status of the semiquinone, its coupling to the iron, its electrostatic environment, and pH-induced structural changes to its site. All of these seem to be related to the ionization of an amino acid group. Moreover, it is possible that the pK_a of this group is influenced by the distant structural effects, which are known to affect the E_m of Q_A/Q_A^-,[46] as well as by the ligands of the nonheme iron which are known to determine the E_m of the Fe^{2+}/Fe^{3+} couple[47] and the photosynthetic electron transfer in the acceptor side of Photosystem II.

Conclusion

This paper introduces the use of the 2D-ESEEM (HYSCORE) spectroscopy as a high-resolution probe of the Q_A^- binding pocket in PSII, which greatly facilitates and improves the analysis of the one-dimensional ESEEM spectra. The present ESEEM and HYSCORE data show that pH is a major factor that modulates the magnetic interactions between the semiquinone radical Q_A^- and protein ^{14}N nuclei. This finding allows a consistent explanation of apparent inconsistencies in previously published data. The present data are interpreted on the basis of a model where the H-bonds to the Q_A^- carbonyls, which are determining factors of these magnetic interactions, are influenced by the presence of the nonheme iron plus a pH-dependent group on the protein. The pK_a of this group varies between 6 and 7.5, depending on the biochemical treatment used to uncouple the iron from the semiquinone. It is suggested that a pH effect on

(44) We note that the ESEEM spectra for Q_A^- iron-depleted PSII published in refs 13 and 22 closely resemble the spectrum in Figure 4 for pH 5.8. This similarity between the ESEEM the high pH-treated PSII with the spectra in PSII samples where the iron is known to be absent corroborates the view that, in high pH-treated PSII, the iron is also absent.

(45) Calvo, R.; Passegi, M. C. G.; Isaacson, R. A.; Okamura, M. Y.; Feher, G. *Biophys. J.* **1995**, *58*, 149.

(46) Krieger, A.; Weiss, E. *Photosynthetica* **1992**, *27*, 89. (b) Krieger A.; Rutherford A. W.; Johnson G. N. *Biochim. Biophys. Acta* **1995**, *1229*, 193. (c) Johnson G. N.; Rutherford A. W.; Krieger A. *Biochim Biophys. Acta* **1995**, *1229*, 202.

(47) Deligiannakis, Y.; Petrouleas, V.; Diner, B. A. *Biochim. Biophys. Acta* **1994**, *1188*, 260. (b) Petrouleas, V.; Deligiannakis, Y.; Diner, B. A. *Biochim. Biophys. Acta* **1994**, *1188*, 271. (c) In an earlier report, Bowden et al. (Bowden, S. J.; Hallahan, B. J.; Ruffle, S. V.; Evans, M. C. W.; Nugent, J. H. A. *Biochim Biophys. Acta* **1991**, *1060*, 89.) had proposed that the magnetic interaction between the semiquinone and the iron is determined by the presence of bound bicarbonate; that is, the "g =1.82" and "g = 1.9" forms of the EPR signal of $Q_A^-Fe^{2+}(S = 2)$ are correlated with the presence and absence, respectively, of bound bicarbonate. However later work in ref 47a,b demonstrated that other anions can substitute bicarbonate in this role and that the carboxylate ligand of the iron determines the pK_a of the ionizable amino acid group that in turn determines the g value of the $Q_A^-Fe^{2+}$ and the E_m of the iron.

the H-bond strength exists in native PSII also and that earlier observations of pH-induced changes in the properties of the semiquinone−iron complex in PSII may reflect this effect. This research provides a basis for the application of 2D-ESEEM for a detailed understanding of the properties of the native semiquinone−iron complex and associated electron-transfer processes in PSII.

Acknowledgment. We would like to thank C. Jegerschöld for her help in the preparation of high pH-treated PSII in the early stages of this study. This work was supported by H.F.S.P.O. Grant RG0349, the E.U. HCM ERBCHRXC940524 Grant, the TMR Grants FMRX-CT96-0031 and FMRX-CT98-0214.

JA984209C